Clinical Oral Investigations (2020) 24:4617–4624
https://doi.org/10.1007/s00784-020-03331-3

ORIGINAL ARTICLE

DNA double-strand breaks of human peripheral blood lymphocyte induced by CT examination of oral and maxillofacial region

Pan Yang[1] · Shuo Wang[1] · Denggao Liu[1] · Hua Zhao[2] · Gang Li[1]

Received: 17 January 2020 / Accepted: 7 May 2020 / Published online: 18 May 2020

Abstract

Objectives To explore whether a computed tomography (CT) examination of the head and neck region induces biological damage and whether the damage was correlated with the radiation dose.

Materials and methods Peripheral blood was taken from 33 individuals who received head and neck CT examinations. Blood samples were divided into three groups: the control group and the in vivo and in vitro irradiation groups. The number of DNA double-strand breaks was estimated by comparing the changes in the rates of γ-H2AX foci formation in the peripheral blood before and after CT examination. The absorbed dose and effective dose were calculated with the software VirtualDose based on the Monte Carlo method, and the absorbed doses in blood were estimated accordingly.

Results The γ-H2AX foci rates were increased in the in vivo ($p < 0.001$) and in vitro irradiation groups ($p < 0.001$) after CT examination when compared with those in the control group. The rate of γ-H2AX foci formation showed linear dose–responses for the CT dose index volume ($CTDI_{vol}$), dose–length product (DLP), and blood dose after CT examination.

Conclusions A CT examination of the head and neck region provides a high enough radiation dose to induce DNA double-strand breaks in cells in the peripheral blood. There was a linear correlation between the formation of DNA double-strand breaks and radiation doses after CT examination.

Clinical relevance In addition to ensuring image quality, in a real clinical situation, the scanning area should be strictly administered, and repeated operations should be avoided to minimise the patient's radiation dose.

Keywords Multidetector computed tomography · Radiation dosage · DNA double-strand break · γ-H2AX

Introduction

It is well-known that acute and delayed effects on human beings can be induced by high-dose radiation, while the amount of damage caused by low doses, which were defined as those of 100 mGy or less by the United Nations Scientific Committee on the Effects of Atomic Radiation (UNSCEAR) in a 2017 report [1], is controversial. According to the linear no-threshold (LNT) model that evolved at the end of the 1950s, every exposure to ionising radiation, no matter how low, constitutes an increased cancer risk [2].

A CT examination is necessary and is commonly used for diagnoses, treatment planning, and prognosis evaluations. With the increased application of CT examination in the head and neck region, potential biological damage has become a public focus, since studies have demonstrated that diagnostic X-rays, including CT scans, may increase cancer risk [3–6].

DNA damage caused by radiation includes DNA double-strand breaks (DSBs), DNA single-strand breaks (SSBs), sugar moiety damage, and base modifications [7]. DSBs are more difficult to repair than other types of DNA damage. SSBs are more easily repaired because only one strand is broken and the other is preserved and could serve as a "template" to repair SSBs [8]. The main methods of the DSB repair pathway include non-homologous end joining (NHEJ) and homologous

Electronic supplementary material The online version of this article (https://doi.org/10.1007/s00784-020-03331-3) contains supplementary material, which is available to authorized users.

✉ Gang Li
kqgang@bjmu.edu.cn

[1] Department of Oral and Maxillofacial Radiology, Peking University School and Hospital of Stomatology & National Engineering Laboratory for Digital and Material Technology of Stomatology & Beijing Key Laboratory of Digital Stomatology, #22 Zhongguancun Nandajie, Hai Dian District, Beijing 100081, China

[2] China CDC Key Laboratory of Radiological Protection and Nuclear Emergency, National Institute for Radiological Protection, Chinese Center for Disease Control and Prevention, Beijing 100088, People's Republic of China

recombination (HR). The NHEJ repair pathway is error-prone because two broken ends of DNA are simply pieced together [9, 10]. If DSBs are not repaired or are repaired incorrectly, it may lead to loss, insertion mutations, and translocations of chromosomes or apoptosis [11, 12]. Inherited defects in DSB repair are implicated in a variety of human pathologies, including increased cancer susceptibility, neurological defects, and/or immunodeficiencies [13]. Therefore, accurately quantifying the amounts of DNA damage, especially DSBs, which are induced by ionising radiation is important to estimate the effects of medical radiation exposure. When DSBs are generated, histone subtype H2A isoform X (H2AX) becomes rapidly phosphorylated at serine 139. The phosphorylated histone subtype H2A isoform X (γ-H2AX) foci that were measured 5 min after in vitro exposure of the blood samples to X-rays increased linearly with the radiation dose. The numbers of foci decreased 5–30 min after irradiation in both the in vivo and in vitro groups, indicating ongoing DSB repair. For all conditions, approximately half of the induced foci were resolved within 30 min after irradiation [14]. Due to the rapid induction and the 1:1 correspondence between the number of γ-H2AX foci and the number of DSBs [15], γ-H2AX-recognising antibodies have become a gold standard to detect the presence of DSBs [16].

Above all, the determination of how to measure radiation dose is a key point to verify the validity of the LNT model. Several parameters can be used to estimate radiation dose. The CT dose index (CTDI) and the dose–length product (DLP) are widely used as the physical exposure parameters of a CT examination. However, both the $CTDI_{vol}$ and DLP are indexes of the radiation output of the CT system, and neither of them directly corresponds with the radiation dose that is delivered to the patient [17]. A practical method for the accurate estimation of the absorbed dose of organs and consequently the effective dose (ED) is the Monte Carlo (MC) method [18–20].

Therefore, the purposes of the present study were:

1) To monitor whether CT examination in the head and neck region induces DNA double-strand breaks
2) To assess the absorbed radiation doses in the blood
3) To investigate whether the DNA double-strand breaks have a relationship with the estimated radiation dose

Materials and methods

Subjects

A total of 33 patients were included. The inclusion criteria were:

1) No habits of smoking and/or drinking
2) No exposure to X-rays in the past three months
3) No recent infection
4) No major systemic diseases, no history of diseases from blood, no surgical history, and no history of systemic medication
5) No history of cancer or radiation therapy

A patient was excluded when one of the above inclusion criteria was not met.

Prior to the CT examination, individual patient information such as age, gender, height and weight, medical history, radiographs exposed, and the exposure parameters were recorded. An informed consent form was signed by the participants or their guardians.

CT examination and blood sample collection

A head and neck CT examination was performed with a 16-slice helical CT scanner (Optima CT 520, GE Healthcare, Waukesha, WI). Prior to the CT examinations, the accuracy and repeatability of the CTDI of the machine were verified. During the CT examinations, a tube voltage of 120 kVp was employed, and the tube current was automatically adjusted according to the patient's condition, giving a range of 80 to 300 mA. The other imaging parameters were as follows: rotation time of 0.8 s, table feed per rotation of 18.75 mm, detector width of 1.25 mm, scan field of view of 25 cm, and matrix of 512 mm. The collimation (beam width) of the CT scan was 20 mm according to the manufacturer's setting, and the pitch was 0.938. The scanning lengths were 14.13–20.37 cm.

Before the CT examination, 10-ml peripheral blood were taken from the elbow vein from each of the patients, and of this, 5 ml was used for the control and 5 ml was used for the in vitro irradiation. After 5 min of the examination, a further 5 ml of blood was taken from the same patient, which was included in the in vivo irradiation group. For in vitro irradiation, the blood was placed next to the patient's head when the patient was exposed to a CT examination. To ensure that the three-dimensional space distances between the blood collection tube and the X-ray tube were consistent, the blood collection tube was put close to the left inner wall of the head positioning device and the long axis of the tube parallel to the *Z*-axis, making the midpoint through the *X*-axis of the positioning line.

Lymphocyte separation and γ-H2AX immunofluorescence analysis

Peripheral blood lymphocyte separation was performed according to the manufacturer's instructions (TDB, Tianjin, China). Two-milliliter fresh heparin anticoagulants were gently overlaid onto 6 ml lymphocyte separation medium. After centrifugation at 400*g* for 20 min, the solution was divided into four layers. The first layer was the plasma. The second layer was the

lymphocytes. The third layer was the lymphocyte separation medium, and the fourth layer was the red blood cells. The second layer of cells was collected and thoroughly mixed in a tube containing 4–5 ml of normal saline for injection. The supernatant was removed after centrifugation at 400*g* for 20 min. The lymphocytes were obtained by two repeated washes.

The separated lymphocytes were fixed in 4% paraformaldehyde (10 min) and permeabilised by 0.1% Triton X-100 (15 min). The samples were incubated with a primary mouse monoclonal anti-H2AX antibody (1:250) (Merck Millipore, Darmstadt, Germany) overnight at 4 °C. After washing in PBS, the lymphocytes were incubated with an Alexa Fluor 488–conjugated goat anti-mouse secondary antibody (1:1000) (Abcam, UK) for 1 h at room temperature. Peripheral blood lymphocytes were again washed and mounted with cover slips using mounting medium with 4′,6-diamidino-2-phenylindole (DAPI).

γ-H2AX foci analysis

The images were taken under a fluorescence microscope at × 400 magnification. We randomly selected at least three visual fields in each of the slices in which the nuclei should be well-dispersed without overlap. In addition, there is no background pollution and no specific fluorescence staining. The total number of cells in the selected visual field of each slice is not less than 100. The nuclei stained by DAPI and the FITC-labelled γ-H2AX foci were photographed.

ImageJ 1.52a (National Institutes of Health, Rockville, MD) was applied for the nuclear detection, quantitative analysis, and identification and number calculation of foci in the nuclei. According to the threshold from the object size and object contrast, the foci signal was extracted from the noise. Detailed information was described in the custom macro program for ImageJ, which is available as Online Resource 1. Three foci with high threshold values were selected, and the average of the threshold values was taken. All images were manually adjusted in this manner to provide an appropriate detection of γ-H2AX foci.

To verify the repeatability, another observer randomly selected ten samples for threshold determination. The γ-H2AX foci rates were calculated by ImageJ and compared with the results of the first observer.

Dose calculation

$CTDI_{vol}$ and DLP were outputted from the CT system. The absorbed dose and ED were calculated by VirtualDose (Virtual Phantoms Inc., Albany, USA), which is a web-based CT organ dose and ED calculator that incorporated 25 "virtual patient" phantoms covering paediatric patients, pregnant patients, normal size adult patients, and overweight adult patients [20]. We chose the most suitable virtual phantoms based on the patient's age, height, and weight. For each patient, anatomical landmarks at the beginning and end of the scan region were used to define the exposed area in the anthropomorphic phantom in VirtualDose. Due to the differences in scan region and the individual differences of the patients, the average mAs per rotation of the scan were not the same. The ED was calculated using tissue weighting factors from the publication ICRP No. 103 that employed a gender-average methodology [21]. The absorbed doses in blood were estimated according to the proposal from Rothkamm et al. [14]. Organ-specific blood volumes were adopted from previously reported reference data [22]. Sex-specific blood volumes and radiation dose calculations were averaged. To obtain the total blood dose, organ-specific doses were weighted according to the blood content in each organ and then summed. The estimated blood dose by organ-specific blood volumes is shown in Table 1.

Statistical analysis

The software package SPSS v16.0 for Windows (SPSS, Chicago, IL, USA) was employed for the statistical analysis. Differences between the frequencies of γ-H2AX foci before and after CT examinations were analysed by Wilcoxon's signed-rank test. Differences between the frequencies of γ-H2AX foci that were obtained by the two observers were analysed by the Wilcoxon signed-rank test. The Friedman signed-rank test was used to analyse the differences among the three sets of sample groups. For the analysis of correlation among different dose levels and foci rates, Spearman's rank correlation was employed. p value < 0.05 was considered significant.

Results

Patients

The study patients consisted of 22 males and 11 females. The age of the patients (means ± SD) was 45.79 ± 12.31 years. The scope of the CT scan ranged from the forehead to the thyroid (4 cases), from the supraorbital ridge to the thyroid (24 cases), from the supraorbital ridge to the clavicle (3 cases), and from the nasion to the thyroid (2 cases).

DLP, $CTDI_{vol}$, ED, and organ dose

The ranges of $CTDI_{vol}$, DLP, ED, and absorbed dose in blood are shown in Table 2. The expected radiation dose in blood calculated with phantom dosimetry ranged from 0.24 to 0.52 mGy.

Table 1 Estimated radiation doses in blood calculated with phantom dosimetry

Organ	Blood volume (100%)*	Radiation dose (mGy)	Blood-weighted dose (mGy)
Adrenal glands	0.1	0.06	0.0001
Bladder	0	0.08	0
Brain	1.2	2.1	0.0252
Gonads	0	0.01	0
Heart	16	0.66	0.1056
Kidneys	2	0.04	0.0008
Liver	10	0.08	0.0080
Lung	12.5	0.78	0.0975
Muscle	12.25	0.37	0.0453
Oesophagus	0.1	1.79	0.0018
Pancreas	0.6	0.11	0.0007
Skin	3	0.44	0.0132
Small intestine	3.8	0.01	0.0004
Spleen	1.4	0.1	0.0014
Stomach	0.9	0.11	0.0010
Thyroid	0.1	4.58	0.0046
Skeleton	7	0.83	0.0581
Lymph nodes	0.2	0.39	0.0008
Fat	6.75	0	0
Large intestine	2.2	0.01	0.0002
Large veins	18	0	0
All other tissues	1.9	1.63	0.0310
All organs	100	…	0.3956

*Contribution of blood in given organ to total blood volume

Changes of γ-H2AX foci

Example images of the observed γ-H2AX foci are shown in Fig. 1. The total number of cells and the foci rate observed in each group of samples are shown in Table 3. The results showed statistically significant differences in cell foci rates among the three groups ($p < 0.001$). The foci rates in the in vivo irradiation group ($p < 0.001$) and the in vitro irradiation group ($p < 0.001$) were significantly increased when compared with those in the control group. In addition, the foci rate in the in vitro group was higher than that in the in vivo group ($p < 0.001$). There was no significant difference between the γ-H2AX foci rates obtained by the two observers ($p = 0.314$).

Table 2 Descriptive data for DLP, $CTDI_{vol}$, ED, and absorbed dose in blood from the 33 subjects

	Minimum	Maximum	Mean	Std. deviation
DLP (mGy·cm)	446.25	905.08	656.83	119.89
$CTDI_{vol}$ (mGy)	25.26	44.21	33.95	4.72
ED (mSv)	0.39	0.80	0.60	0.11
Blood (mGy)	0.24	0.52	0.38	0.08

CT, computed tomography; *DLP*, dose–length product; $CTDI_{vol}$, computed tomography dose index (volume); *ED*, effective dose

Dose–response correlation analysis

The rate of γ-H2AX foci in the in vivo irradiation group showed a linear dose–response with the blood dose ($p < 0.001$, $\rho = 0.684$). Additionally, the rate of γ-H2AX foci in the in vitro irradiation group showed a linear dose–response with the $CTDI_{vol}$ ($p < 0.001$, $\rho = 0.840$) and DLP ($p < 0.001$, $\rho = 0.771$). The results are shown in Fig. 2.

Discussion

Diagnostic reference values are widely applied in many countries. According to the literature, for adult head CT examinations, the $CTDI_{vol}$ values are from 49 to 70 mGy, and DLP values are from 733 to 1312 mGy·cm [23–25]. The $CTDI_{vol}$ (25.26–44.21 mGy) and DLP (446.25–905.08 mGy·cm) values presented in the current study were just within the range.

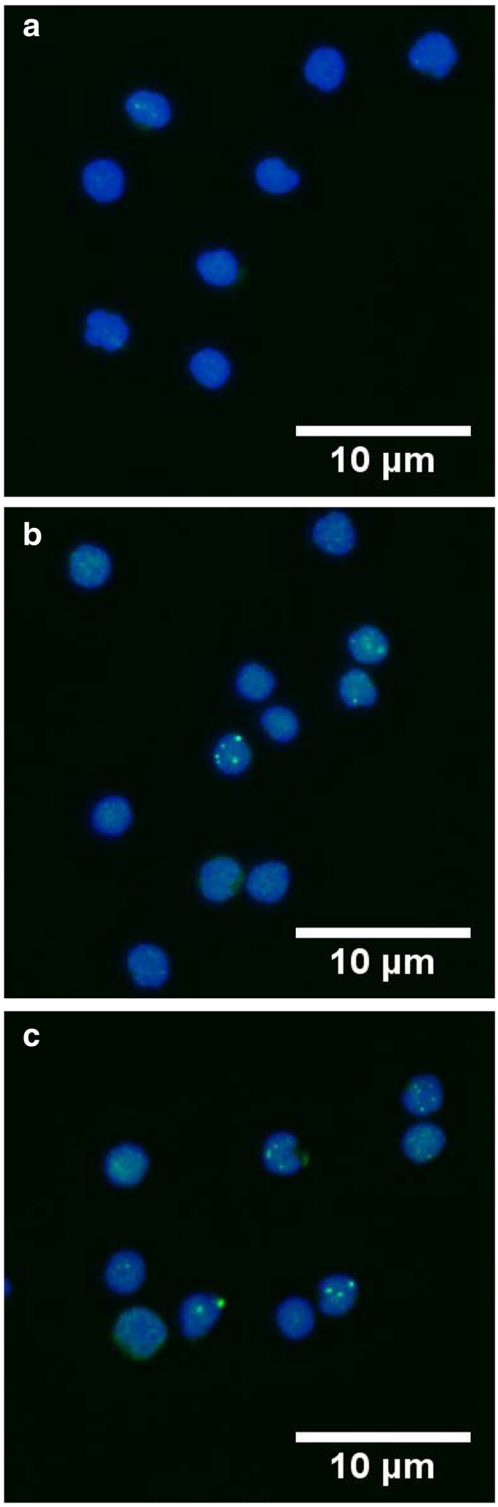

Fig. 1 Examples of images of the observed γ-H2AX foci in the peripheral blood lymphocyte nuclei in the control (**a**), in vivo (**b**), and in vitro (**c**) groups

In the present study, γ-H2AX foci were increased in both in vivo and in vitro blood samples after CT examination, and the increase in γ-H2AX foci has a linear relationship with the radiation dose. Similar results were found in other studies [26–28]. In the study by Fukumoto et al., the γ-H2AX foci were significantly correlated with CTDI, DLP, and size-

Table 3 Sample size, observed cells, detection number of aberration, and the mean rate of detected aberration of the γ-H2AX assay

	Control	In vivo	In vitro
Cells observed	15258	14143	16028
Aberration detection number	2602	5281	8454
Mean rate of detected aberration	0.171	0.373	0.527

γ-H2AX, phosphorylated histone subtype H2A isoform X

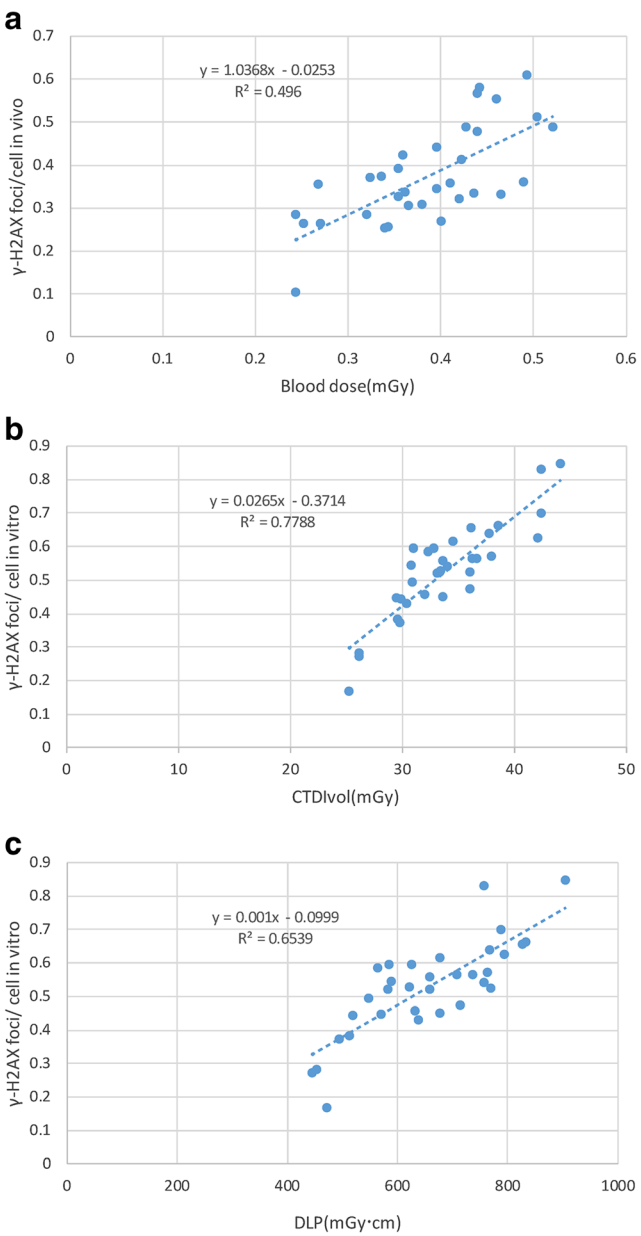

Fig. 2 Linear relationship between the γ-H2AX foci rate and blood doses (**a**), CT dose index volume ($CTDI_{vol}$) in the in vitro irradiation group (**b**), and dose length–product (DLP) in the in vitro irradiation group (**c**)

specific dose estimate [26]. In the study by Lobrich et al., the linear relationship between γ-H2AX foci number and DLP further suggests that the thorax/abdomen exposures produce similar numbers of foci for the same delivered doses. A CT of the head, by contrast, induces significantly fewer foci [28]. However, a big difference of the present study with others for the head and neck CT examinations is that the radiation dose in the blood was calculated and used for analysis in the in vivo conditions.

We checked the literature and only found two studies using blood dose for the analysis of dose–response. In the study by Vandevoorde et al. [29], the blood doses of 51 paediatric patients who received abdomen or chest CT examinations were estimated and used for the analysis of relationship between radiation doses and induced γ-H2AX foci. The estimated blood doses were 0.14–2.84 mGy for the chest and 0.66–8.85 for the abdomen CT scans. The results indicate that the induced γ-H2AX foci initially show a sharp increase within the doses of 2 mGy and then appear a bit flat. Similarly, in the study by Beels et al. [30], a biphasic trend line was drawn that the radiation-induced γ-H2AX foci have a steep linear increase up to 10 mGy followed by a more flat increase at higher doses. The estimated blood doses were 0.24–0.52 mGy in the present study and just fell in the linear response range of the studies.

$CTDI_{vol}$ and DLP are good measurements for doses during CT examinations. However, without consideration of patient size and the real heterogeneous attenuation of individuals, they are only representations of the dose outside the patient rather than a real dose to patient. This is why we only use $CTDI_{vol}$ and DLP for the correlation analyses among doses and the γ-H2AX foci rate in the in vitro groups. According to the review of patient doses from CT examinations in the UK for 2003, the mean $CTDI_{vol}$ and DLP of routine head scans were slightly higher than those of chest CT and abdomen CT, but with respect to mean ED, the routine head CT was lower. This might explain why the thorax and abdomen CT examination produced more γ-H2AX foci than the skull CT examination at the same dose of DLP [28].

VirtualDose is the first online absorbed dose and ED calculator that incorporates anatomically realistic phantoms for patients of various ages, gender, pregnancy stages, or body sizes [20]. To obtain a more accurate organ dose in the in vivo condition, we recorded the scanned upper and lower borders of a patient since doses to the organs are sensitive to changes of scan range by centimetres or even by millimetres. For example, a 3-cm extension can increase the dose to the salivary glands by more than 2 times [31].

The results of the present study showed that the γ-H2AX foci rate in the in vitro group was higher than that in the in vivo irradiation group. This is logical, since all of the blood in the in vitro irradiation group were exposed to the full level of radiation from the CT examination, while the blood in the in vivo group were exposed to only a part of the radiation in the blood circulating through the whole body. Therefore, the blood dose of the in vivo irradiation group was relatively less than that of the in vitro irradiation group.

This study has some limitations. First, our experiment was sampled from human peripheral blood. In the CT examination of the head and neck region, the patient's crystalline lens, thyroid, and oral salivary glands are the most sensitive organs to radiation. However, it is not possible to take samples from these organs to observe the biological effects. Second, changes in peripheral blood lymphocytes were monitored only 5 min after the CT examination. The repair ability and the long-term effects of DSBs in the human body have not been observed, so we do not know whether the biological effects still exists after 0.5 h and 6 h or even after a longer period of time. Studies have shown that the frequencies of γ-H2AX foci are related to decreases with time. In the in vitro study by Popp et al. [32], the number of γ-H2AX foci peaked at 5 min, then decreased rapidly for 5 h and repaired slowly until 24 h after a CT examination at absorbed doses of 3 mGy, 15 mGy, and 50 mGy. In the study by Kuefner et al. [33], a single irradiation with 50 mGy led to a maximum of DSBs 15 min after exposure, and approximately two-thirds of these DNA lesions disappeared within 2.5 h in the in vivo and in vitro irradiation groups. According to the results of the study by Rothkamm et al. [14], half of the induced foci were resolved within 30 min in the in vivo and in vitro irradiation groups after exposure. Therefore, we should consider how much time should be allowed between different X-ray examinations to allow for repair and to avoid the cumulative effect of radiation. Third, even though we calculated the patient's absorbed dose through the VirtualDose program, it is still a calculation from 25 virtual phantoms and not real patients. The patient's individual condition cannot be completely and accurately reflected. Fourth, the position of the in vitro sample next to the patient head plays a key role in the radiation dose that has been delivered to the sample. To minimise possible influence from distances, the blood collection tube was fixed in such a way that the three-dimensional space distance between the centre of the blood tube and the X-ray tube was kept consistent. Fifth, although there was no difference between the two observers in the present study, the observed foci numbers varied between laboratories, despite using a standard protocol from the study by Moquet et al. [34]. The possible causes for this are the small variations in the treatment of samples, laboratory reagents from different suppliers, etc.

Based on the results of the present study, it can be concluded that a CT examination of the head and neck region can cause DNA double-strand breaks in the peripheral blood lymphocytes. There was a significant correlation between the exposed doses and DNA double-strand breaks.

Implications for the clinic

A CT examination is necessary and is commonly used for diagnoses, treatment planning, and prognosis evaluations in diseases of the head and neck region. The study is helpful for clinicians and patients to understand the potential biological damage of CT examinations in the head and neck area. In addition to ensuring image quality in a real clinical situation, the scanning area should be strictly administered, and repeated operations should be avoided to minimise the patient's radiation dose.

Funding information This study has received funding from the National Natural Science Foundation of China (No. 81671034) and National Key R&D Program of China (No. 2018YFC0807303)

Compliance with ethical standards

Conflict of interest The authors declare that they have no conflict of interest.

Ethical approval All procedures performed in studies involving human participants were in accordance with the ethical standards of the institutional and/or national research committee and with the 1964 Helsinki declaration and its later amendments or comparable ethical standards. The study was approved by the Institutional Review Board of Peking University School and Hospital of Stomatology (PKUSSIRB-201944052).

Informed consent Informed consent was obtained from all individual participants included in this study. They received oral and written information about the design of the study and their right to withdraw at any time without negative effect on their treatment.

References

1. UNSCEAR (2018) Sources, effects and risks of ionizing radiation, Annex B. Epidemiological studies of cancer risk due to low-dose-rate radiation from environmental sources. UNSCEAR Publications. https://www.unscear.org/unscear/en/publications/2017.html. Accessed 30 March 2018
2. Calabrese EJ (2013) Origin of the linearity no threshold (LNT) dose-response concept. Arch Toxicol 87(9):1621–1633. https://doi.org/10.1007/s00204-013-1104-7
3. Shah DJ, Sachs RK, Wilson DJ (2012) Radiation-induced cancer: a modern view. Br J Radiol 85(1020):e1166–e1173. https://doi.org/10.1259/bjr/25026140
4. Brenner DJ (2004) Radiation risks potentially associated with low-dose CT screening of adult smokers for lung cancer. Radiology 231(2):440–445. https://doi.org/10.1148/radiol.2312030880
5. Brenner DJ, Elliston CD (2004) Estimated radiation risks potentially associated with full-body CT screening. Radiology 232(3):735–738. https://doi.org/10.1148/radiol.2323031095
6. Berrington de Gonzalez A, Darby S (2004) Risk of cancer from diagnostic X-rays: estimates for the UK and 14 other countries. Lancet 363(9406):345–351. https://doi.org/10.1016/s0140-6736(04)15433-0
7. Friedberg EC, Walker GC, Siede W, Wood RD, Schultz RA, Ellenberger T. (2006) DNA repair and mutagenesis, Washington
8. Tuteja N, Tuteja R (2001) Unraveling DNA repair in human: molecular mechanisms and consequences of repair defect. Crit Rev Biochem Mol Biol 36(3):261–290. https://doi.org/10.1080/20014091074192
9. Lieber MR, Ma Y, Pannicke U, Schwarz K (2004) The mechanism of vertebrate nonhomologous DNA end joining and its role in V(D)J recombination. DNA Repair (Amst) 3(8–9):817–826. https://doi.org/10.1016/j.dnarep.2004.03.015
10. Burma S, Chen BPC, Chen DJ (2006) Role of non-homologous end joining (NHEJ) in maintaining genomic integrity. DNA Repair (Amst) 5:1042–1048. https://doi.org/10.1016/j.dnarep.2006.05.026
11. Rich T, Allen RL, Wyllie AH (2000) Defying death after DNA damage. Nature 407(6805):777–783. https://doi.org/10.1038/35037717
12. Hoeijmakers JH (2009) DNA damage, aging, and cancer. N Engl J Med 361(15):1475–1485. https://doi.org/10.1056/NEJMra0804615
13. McKinnon PJ (2012) ATM and the molecular pathogenesis of ataxia telangiectasia. Annu Rev Pathol 7:303–321. https://doi.org/10.1146/annurev-pathol-011811-132509
14. Rothkamm K, Balroop S, Shekhdar J, Fernie P, Goh V (2007) Leukocyte DNA damage after multi-detector row CT: a quantitative biomarker of low-level radiation exposure. Radiology 242(1):244–251. https://doi.org/10.1148/radiol.2421060171
15. Sedelnikova OA, Rogakou EP, Panyutin IG, Bonner WM (2002) Quantitative detection of (125)IdU-induced DNA double-strand breaks with gamma-H2AX antibody. Radiat Res 158(4):486–492. https://doi.org/10.1667/0033-7587(2002)158[0486:qdoiid]2.0.co;2
16. Fernandez-Capetillo O, Lee A, Nussenzweig M, Nussenzweig A (2004) H2AX: the histone guardian of the genome. DNA Repair (Amst) 3(8–9):959–967. https://doi.org/10.1016/j.dnarep.2004.03.024
17. McCollough CH, Leng S, Yu L, Cody DD, Boone JM, McNitt-Gray MF (2011) CT dose index and patient dose: they are not the same thing. Radiology 259(2):311–316. https://doi.org/10.1148/radiol.11101800
18. Turner AC, Zhang D, Khatonabadi M, Zankl M, DeMarco JJ, Cagnon CH, Cody DD, Stevens DM, McCollough CH, McNitt-Gray MF (2011) The feasibility of patient size-corrected, scanner-independent organ dose estimates for abdominal CT exams. Med Phys 38(2):820–829. https://doi.org/10.1118/1.3533897
19. Lee C, Kim KP, Long DJ, Bolch WE (2012) Organ doses for reference pediatric and adolescent patients undergoing computed tomography estimated by Monte Carlo simulation. Med Phys 39(4):2129–2146. https://doi.org/10.1118/1.3693052
20. Ding A, Gao Y, Liu H, Caracappa PF, Long DJ, Bolch WE, Liu B, Xu XG (2015) VirtualDose: a software for reporting organ doses from CT for adult and pediatric patients. Phys Med Biol 60(14):5601–5625. https://doi.org/10.1088/0031-9155/60/14/5601
21. ICRP (2007) The 2007 Recommendations of the International Commission on Radiological Protection. ICRP publication 103. Ann ICRP 37(2–4):1–332. https://doi.org/10.1016/j.icrp.2007.10.009
22. ICRP (2002) Basic anatomical and physiologic data for use in radiological protection: reference values—a report of age- and genderrelated differences in the anatomical and physiological characteristics of reference individuals. ICRP publication no. 89. Ann ICRP 32:5–265. https://doi.org/10.1016/S0146-6453(03)00002-2
23. Shrimpton PC, Hillier MC, Lewis MA, Dunn M (2006) National survey of doses from CT in the UK: 2003. Br J Radiol 79(948):968–980. https://doi.org/10.1259/bjr/93277434
24. Atac GK, Parmaksiz A, Inal T, Bulur E, Bulgurlu F, Oncu T, Gundogdu S (2015) Patient doses from CT examinations in Turkey. Diagn Interv Radiol 21(5):428–434. https://doi.org/10.5152/dir.2015.14306
25. Chinese Society of Image Quality Control And Safety (2017) Diagnostic Reference levels for CT examinations: an expert

consensus. Chin J Radiol 51(11):817–822. https://doi.org/10.3760/cma.j.issn.1005?1201.2017.11.001 (In Chinese)
26. Fukumoto W, Ishida M, Sakai C, Tashiro S, Ishida T, Nakano Y, Tatsugami F, Awai K (2017) DNA damage in lymphocytes induced by cardiac CT and comparison with physical exposure parameters. Eur Radiol 27(4):1660–1666. https://doi.org/10.1007/s00330-016-4519-8
27. Kuefner MA, Brand M, Engert C, Schwab SA, Uder M (2015) Radiation induced DNA double-strand breaks in radiology. Rofo 187(10):872–878. https://doi.org/10.1055/s-0035-1553209
28. Lobrich M, Rief N, Kuhne M, Heckmann M, Fleckenstein J, Rube C, Uder M (2005) In vivo formation and repair of DNA double-strand breaks after computed tomography examinations. Proc Natl Acad Sci U S A 102(25):8984–8989. https://doi.org/10.1073/pnas.0501895102
29. Vandevoorde C, Franck C, Bacher K, Breysem L, Smet MH, Ernst C, de Backer A, van de Moortele K, Smeets P, Thierens H (2015) gamma-H2AX foci as in vivo effect biomarker in children emphasize the importance to minimize x-ray doses in paediatric CT imaging. Eur Radiol 25(3):800–811. https://doi.org/10.1007/s00330-014-3463-8
30. Beels L, Bacher K, Smeets P, Verstraete K, Vral A, Thierens H (2012) Dose-length product of scanners correlates with DNA damage in patients undergoing contrast CT. Eur J Radiol 81(7):1495–1499. https://doi.org/10.1016/j.ejrad.2011.04.063
31. Gao Y, Quinn B, Mahmood U, Long D, Erdi Y, St. Germain J, Pandit-Taskar N, Xu XG, Bolch WE, Dauer LT (2017) A comparison of pediatric and adult CT organ dose estimation methods. BMC Med Imaging 17(1):28. https://doi.org/10.1186/s12880-017-0199-3
32. Popp HD, Meyer M, Brendel S, Prinzhorn W, Naumann N, Weiss C, Seifarth W, Schoenberg SO, Hofmann WK, Henzler T, Fabarius A (2016) Leukocyte DNA damage after reduced and conventional absorbed radiation doses using 3rd generation dual-source CT technology. Eur J Radiol Open 3:134–137. https://doi.org/10.1016/j.ejro.2016.06.001
33. Kuefner MA, Grudzenski S, Schwab SA, Wiederseiner M, Heckmann M, Bautz W, Lobrich M, Uder M (2009) DNA double-strand breaks and their repair in blood lymphocytes of patients undergoing angiographic procedures. Invest Radiol 44(8):440–446. https://doi.org/10.1097/RLI.0b013e3181a654a5
34. Moquet J, Barnard S, Staynova A, Lindholm C, Monteiro Gil O, Martins V, Rößler U, Vral A, Vandevoorde C, Wojewódzka M, Rothkamm K (2017) The second gamma-H2AX assay intercomparison exercise carried out in the framework of the European biodosimetry network (RENEB). Int J Radiat Biol 93(1):58–64. https://doi.org/10.1080/09553002.2016.1207822